

Short-distance propagation of nonlinear optical pulses

Mathieu Isoard¹, A. M. Kamchatnov^{2,3} & N. Pavloff¹

¹ LPTMS, UMR 8626, CNRS, Univ. Paris-Sud, Université Paris-Saclay, 91405 Orsay, France

² Institute of Spectroscopy, Russian Academy of Sciences, Troitsk, Moscow, 108840, Russia

³ Moscow Institute of Physics and Technology, Institutsky lane 9, Dolgoprudny, Moscow region, 141701, Russia
mathieu.isoard@u-psud.fr

Résumé. Nous étudions la propagation transverse d'un pulse lumineux quasi-unidimensionnel dans un milieu optique non-linéaire, en présence d'un fond d'intensité lumineuse constante. Dans un premier temps, le signal initial se divise en deux parties qui se propagent dans des directions opposées. Ce phénomène peut être décrit théoriquement à l'aide d'une approche non dispersive en utilisant une modification de la méthode de Riemann proposée par Ludford. Les résultats sont en excellent accord avec les simulations numériques.

Abstract. We theoretically describe the quasi one-dimensional transverse spreading of a light pulse propagating in a defocusing nonlinear optical material in the presence of a uniform background light intensity. For short propagation distances the pulse can be described within a nondispersive approximation by means of Riemann's approach. The theoretical results are in excellent agreement with numerical simulations.

1 Introduction

It has long been realized that light propagating in a nonlinear medium was amenable to a hydrodynamic treatment [1,2]. In the present work we use such an approach to study a model configuration which has been realized experimentally in a one-dimensional situation in the defocusing regime in Ref. [3]: the nonlinear spreading of a region of increased light intensity in the presence of a uniform constant background. In the absence of background, and for a smooth initial intensity pattern, the spreading is mainly driven by the nonlinear defocusing and can be treated analytically in some simple cases [1]. The situation is more interesting in the presence of a constant background: the pulse splits in two parts, each eventually experiencing nonlinear wave breaking, leading to the formation of dispersive shock waves at both extremities of the split pulse. In the present work we concentrate on the pre-shock period and demonstrate that it can be very accurately described within a non-dispersive nonlinear approximation.

The paper is organized as follows: In Sec. 2 we present the model and the set-up we aim at studying. The spreading and the splitting stage of evolution is accounted for in Sec. 3 within a dispersionless approximation which holds when the pulse region initially presents no large intensity gradient. The problem is first mapped onto an Euler-Poisson equation in Sec. 3.1. This equation is solved in Sec. 3.2 by using Riemann-Ludford method. In Sec. 3.3 the theoretical results are compared with numerical simulations. Our conclusions are presented in Sec. 4.

2 The model

In the paraxial approximation, the stationary propagation of the complex amplitude $A(\mathbf{r})$ of the electric field of a monochromatic beam is described by the equation (see, e.g., Ref. [4])

$$i\partial_z A = -\frac{1}{2n_0 k_0} \nabla_{\perp}^2 A - k_0 \delta n A .$$

In this equation, n_0 is the linear refractive index, $k_0 = 2\pi/\lambda_0$ is the carrier wave vector, z is the longitudinal coordinate along the beam, ∇_{\perp}^2 the transverse Laplacian and δn is a nonlinear contribution to the index. In a non absorbing defocusing Kerr nonlinear medium one can write $\delta n = -n_2 |A|^2$, with $n_2 > 0$.

We consider a system with a uniform background light intensity, denoted as I_0 , on top of which an initial pulse is added at the entrance of the nonlinear cell. To study the propagation of this pulse along the beam (direction z), we introduce the following characteristic quantities: the nonlinear length $z_{\text{NL}} = (k_0 n_2 I_0)^{-1}$ and the transverse healing length $\beta_{\perp} = (z_{\text{NL}}/n_0 k_0)^{1/2}$. Since the transverse profile depends on a single Cartesian coordinate, we write $\nabla_{\perp}^2 = \beta_{\perp}^{-2} \partial_x^2$ where x is the dimensionless transverse coordinate, and also define an effective “time” $t = z/z_{\text{NL}}$. In this framework, the quantity $\psi(x, t) = A(x, t)/\sqrt{I_0}$ is solution of the dimensionless nonlinear Schrödinger (NLS) equation

$$i\psi_t = -\frac{1}{2}\psi_{xx} + |\psi|^2\psi. \quad (1)$$

The initial $\psi(x, t = 0)$ is real (i.e., no transverse velocity or, in optical context, no focusing of the light beam at the input plane), with a dimensionless intensity $\rho(x, t) = |\psi|^2$ which departs from the constant background value (which we denote as ρ_0) only in the region near the origin where it forms a bump. To be specific, we consider the typical case where

$$\rho(x, 0) = \rho_0 + \rho_1 \exp(-2x^2/x_0^2), \quad \text{and} \quad u(x, 0) = 0. \quad (2)$$

The maximal density of the initial profile is $\rho(0, 0) = \rho_0 + \rho_1 \equiv \rho_m$.

3 The dispersionless stage of evolution

The initial pulse splits into two signals propagating in opposite directions of x axis. The aim of this section is to theoretically describe this splitting within a dispersionless approximation.

3.1 Riemann variables and Euler-Poisson equation

By means of the Madelung substitution $\psi(x, t) = \sqrt{\rho(x, t)} \exp(i \int^x u(x', t) dx')$, the NLS equation (1) can be cast into a hydrodynamic-like form for the density $\rho(x, t)$ and the flow velocity $u(x, t)$:

$$\rho_t + (\rho u)_x = 0, \quad u_t + uu_x + \rho_x + \left(\frac{\rho_x^2}{8\rho^2} - \frac{\rho_{xx}}{4\rho} \right)_x = 0. \quad (3)$$

These equations are to be solved with the initial conditions (2). The last term of the left hand-side of the second of Eqs. (3) accounts for the dispersive character of the fluid of light. In the first stage of spreading of the bump, if the density gradients of the initial density are weak (i.e., if $x_0 \gg \min\{\rho_0^{-1/2}, \rho_1^{-1/2}\}$), the effects of dispersion can be neglected, and the system (3) simplifies to

$$\rho_t + (\rho u)_x = 0, \quad u_t + uu_x + \rho_x = 0. \quad (4)$$

The above equations can be written in a more symmetric form by introducing the Riemann invariants

$$\lambda^{\pm}(x, t) = \frac{1}{2}u(x, t) \pm \sqrt{\rho(x, t)}, \quad (5)$$

which evolve according to the system [equivalent to (4)]:

$$\partial_t \lambda^{\pm} + v_{\pm}(\lambda^-, \lambda^+) \partial_x \lambda^{\pm} = 0, \quad \text{with} \quad v_{\pm}(\lambda^-, \lambda^+) = \frac{1}{2}(3\lambda^{\pm} + \lambda^{\mp}) = u \pm \sqrt{\rho}. \quad (6)$$

The Riemann velocities v_{\pm} in (6) have a simple physical interpretation for a smooth velocity and density distribution: v_+ (v_-) corresponds to a signal which propagates downstream (upstream) at the local velocity of sound $c = \sqrt{\rho}$ and which is dragged by the background flow u .

The system (6) can be linearized by means of the hodograph transform (see, e.g., Ref. [5]) which consists in considering x and t as functions of λ^+ and λ^- . One readily obtains

$$\partial_{\pm} x - v_{\mp} \partial_{\pm} t = 0, \quad (7)$$

where $\partial_{\pm} \equiv \partial/\partial\lambda^{\pm}$. One introduces two auxiliary (yet unknown) functions $W_{\pm}(\lambda^{-}, \lambda^{+})$ such that

$$x - v_{\pm}(\lambda^{-}, \lambda^{+})t = W_{\pm}(\lambda^{-}, \lambda^{+}). \quad (8)$$

Inserting the above expressions in (7) shows that the W_{\pm} 's are solution of Tsarev equations [6]

$$\frac{\partial_{-}W_{+}}{W_{+} - W_{-}} = \frac{\partial_{-}v_{+}}{v_{+} - v_{-}}, \quad \text{and} \quad \frac{\partial_{+}W_{-}}{W_{+} - W_{-}} = \frac{\partial_{+}v_{-}}{v_{+} - v_{-}}. \quad (9)$$

From Eqs. (6) and (9) one can verify that $\partial_{-}W_{+} = \partial_{+}W_{-}$, which shows that W_{+} and W_{-} can be sought in the form

$$W_{\pm} = \partial_{\pm}\chi, \quad (10)$$

where $\chi(\lambda^{-}, \lambda^{+})$ plays the role of a potential. Substituting expressions (10) in one of the Tsarev equations shows that χ is a solution of the following Euler-Poisson equation

$$\frac{\partial^2\chi}{\partial\lambda^{+}\partial\lambda^{-}} - \frac{1}{2(\lambda^{+} - \lambda^{-})} \left(\frac{\partial\chi}{\partial\lambda^{+}} - \frac{\partial\chi}{\partial\lambda^{-}} \right) = 0. \quad (11)$$

3.2 Solution of the Euler-Poisson equation

We use Riemann's method (see, e.g., Ref. [7]) to solve the Euler-Poisson equation (11) in the $(\lambda^{+}, \lambda^{-})$ -plane which we denote below as the ‘‘characteristic plane’’. We follow here the procedure exposed in Ref. [8] which applies to non-monotonous initial distributions, such as the one corresponding to Eq. (2).

We first schematically depict in Fig. 1(a) the initial spatial distributions $\lambda^{\pm}(x, 0)$ of the Riemann invariants (left panel). The initial condition (2) yields $\lambda^{\pm}(x, 0) = \pm\sqrt{\rho(x, 0)}$. A later stage of evolution is shown in the right panel of Fig. 1. We introduce notations for some remarkable values of the Riemann invariants: $\lambda^{\pm}(-\infty, t) = \lambda^{\pm}(\infty, t) = \pm\sqrt{\rho_0} \equiv \pm c_0$ and $\lambda^{\pm}(0, 0) = \pm\sqrt{\rho_m} \equiv \pm c_m$. We also define as part A (part B) the branch of the distribution of the λ^{\pm} 's which is at the right (at the left) of the extremum $\pm c_m$. These notations are summarized in Fig. 1(a).

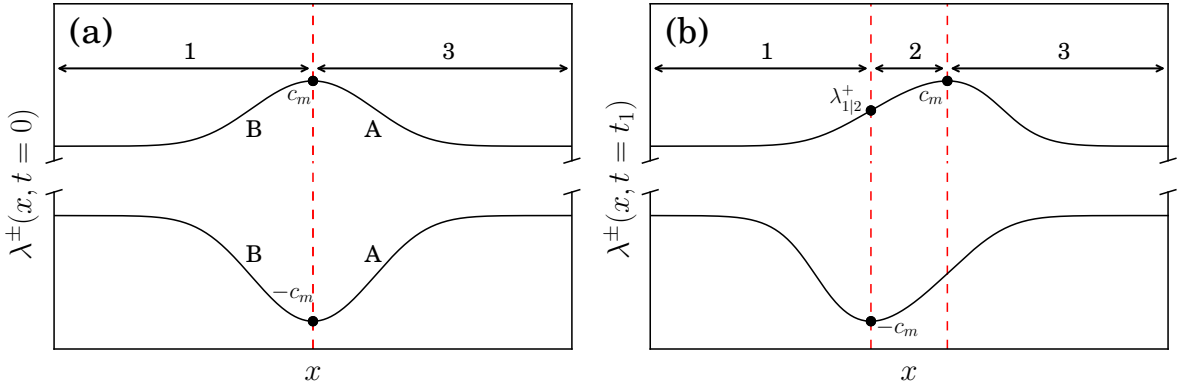


Figure 1. Sketch of the distributions $\lambda^{\pm}(x, t)$ at time $t = 0$ (left panel) and at finite time $t > 0$ (right panel). In each panel the upper solid curve represent λ^{+} (always larger than c_0), and the lower one λ^{-} (always lower than $-c_0$). Panel (a) corresponds to the initial distribution, in which part B corresponds to region 1 and part A to region 3 (see the text). For $t > 0$, λ^{+} (λ^{-}) moves to the right (to the left) and part B of λ^{+} starts to overlap with part A of λ^{-} . This leads to the configuration represented in panel (b) where a new region (labeled region 2) has appeared. For later convenience, the value $\lambda_{1|2}^{+}(t_1)$ is added in this panel. It corresponds to the value of λ^{+} at the boundary between regions 1 and 2 (see the discussion in Sec. 3.3).

At a given finite time, the x axis can be considered as divided in three domains, each requiring a specific treatment. Each domain is characterized by the behavior of the Riemann invariants. In domain

3 (domain 1 respectively), λ^+ is decreasing (increasing) while λ^- is increasing (decreasing); in domain 2 both are increasing, see Fig. 1(b). The theoretical description of this nonlinear wave is challenging because in each regions *both* Riemann invariants (λ^+ and λ^-) depend on position (i.e., there is no simple wave region).

The values of the Riemann invariants corresponding to Fig. 1(b) are represented in the characteristic plane in Fig. 2(a). The red curve \mathcal{C}^0 in Figs. 2(a) and (b) corresponds to the initial conditions depicted in Fig. 1(a). Since $\lambda^+(x, 0) = -\lambda^-(x, 0)$, the curve \mathcal{C}^0 lies along the anti-diagonal in the characteristic plane. The (blue) curvy lines correspond to regions where both Riemann invariants depend on position: the domains 1, 2 and 3. In each of these three domains the solution χ of the Euler-Poisson equation has a different expression. In order to describe these three branches, following Ludford [8], we introduce several sheets in the characteristic plane by unfolding the domain $[c_0, c_m] \times [-c_m, -c_0]$ into a four times larger region as illustrated in Fig. 2(b). We remark here that the whole region above \mathcal{C}^0 — shaded in Fig. 2(b) — is unreachable for the initial distribution we consider: for instance, the upper shaded triangle in region 1 would correspond to a configuration in which $\lambda_{\text{region1}}^+(x, t) > |\lambda_{\text{region1}}^-(x, t)|$, which does not occur in our case, see Fig. 1(b). The potential $\chi(\lambda^-, \lambda^+)$ can now take a different form in each of the regions labeled as 1, 2 and 3 in Fig. 2(b) and still be considered as single-valued. In each of the three domains, we use Riemann-Ludford method to solve Eq. (11). This yields, to a very good approximation (a thorough analysis can be found in Ref. [9])

$$\chi^{(n)}(\lambda^-, \lambda^+) = \frac{\sqrt{2}}{\sqrt{\lambda^+ - \lambda^-}} \int_{-\lambda^-}^{\lambda^+} \sqrt{r} w^{A/B}(r) dr, \quad (12)$$

for regions $n = 1$ and 3. In the above formula, the superscript A should be used when $n = 3$, and the superscript B when $n = 1$, and w^A (w^B) is the inverse function of the initial λ profiles in part A (part B). For the initial condition (2) one has

$$x = w^{A/B}(\lambda) = \pm x_0 \sqrt{-\frac{1}{2} \ln \frac{\lambda^2 - \rho_0}{\rho_1}} \quad \text{if } x \geq 0.$$

In region 2, the formulae (12) are replaced by

$$\chi^{(2)}(\lambda^-, \lambda^+) = \frac{\sqrt{2}}{\sqrt{\lambda^+ - \lambda^-}} \left(\int_{c_m}^{\lambda^+} \sqrt{r} w^B(r) dr + \int_{-\lambda^-}^{c_m} \sqrt{r} w^A(r) dr \right). \quad (13)$$

3.3 Results and comparison with numerical simulations

Once $\chi^{(n)}(\lambda^-, \lambda^+)$ has been determined in each of the three regions ($n = 1, 2$ or 3), the problem is solved. One first computes $W_{\pm}^{(n)}(\lambda^-, \lambda^+)$ in each region from Eqs. (10), (12) and (13). Then, the procedure to obtain the values of λ^{\pm} and λ^- as functions of x and t is the following:

- One starts by determining the value of λ^+ for which $\lambda^- = -c_m$ at time t . This value of λ^+ defines the boundary between regions 1 and 2. We denoted it as $\lambda_{1|2}^+(t)$; it is represented in Fig. 1(b). From Eqs. (8), $\lambda_{1|2}^+(t)$ is a solution of

$$\frac{W_+^{(1)}(-c_m, \lambda_{1|2}^+) - W_-^{(1)}(-c_m, \lambda_{1|2}^+)}{v_+(-c_m, \lambda_{1|2}^+) - v_-(-c_m, \lambda_{1|2}^+)} + t = 0. \quad (14)$$

We then know that, in region 1 at time t , λ^+ takes all possible values between c_0 and $\lambda_{1|2}^+(t)$.

- One picks a value of λ^+ in $[c_0, c_m]$. From Eqs. (8), λ^- is then solution of

$$\frac{W_+^{(n)}(\lambda^-, \lambda^+) - W_-^{(n)}(\lambda^-, \lambda^+)}{v_+(\lambda^-, \lambda^+) - v_-(\lambda^-, \lambda^+)} + t = 0, \quad (15)$$

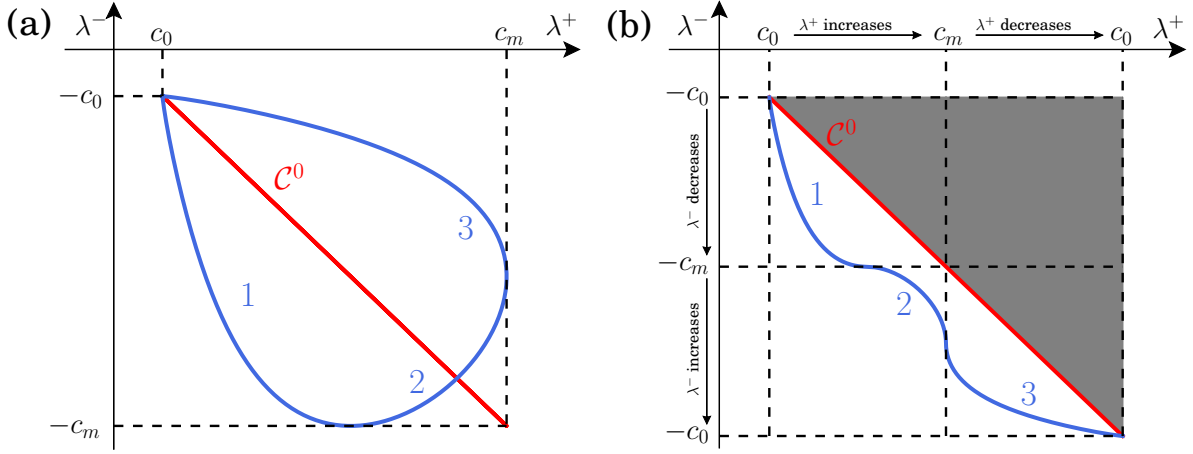


Figure 2. (a) Behavior of the Riemann invariants in the characteristic plane at a given time t (blue curve). The red curve \mathcal{C}^0 corresponds to the initial condition $[\lambda^-(x, 0) = -\lambda^+(x, 0)]$. (b) The same curves in the four-sheeted unfolded surface. In our problem, the whole grey shaded domain above \mathcal{C}^0 is unreachable.

with $n = 1$ if $\lambda^+ \in [c_0, \lambda_{1|2}^+(t)]$ and $n = 2$ if $\lambda^+ \in [\lambda_{1|2}^+(t), c_m]$. This determines the value of the Riemann invariants in regions 1 and 2. In region 3 one uses the symmetry of the problem and writes $\lambda^\pm(x, t) = -\lambda^\mp(-x, t)$, see Fig. 1(b).

- At this point, for each value of t and λ^+ we know the value of the other Riemann invariant λ^- . The position x is then simply obtained by either one of Eqs. (8). So, for given t and λ^+ in region n , one has determined the values of λ^- and x . In practice, this makes it possible to associate a couple (λ^-, λ^+) to each (x, t) . The density and velocity profiles are then obtained through Eqs. (5).

The results of the above approach are compared in Fig. 3 with the numerical solution of Eq. (1), taking the initial condition given by Eq. (2) with $\rho_0 = 0.5$, $\rho_1 = 1.5$ and $x_0 = 20$. One reaches an excellent agreement for the density profile and also for the velocity profile (not shown in the figure) up to $t \simeq 20$. As time increases, the profile steepens and oscillations become visible at both ends of the pulse at $t \gtrsim 16$. There exists a certain time, the wave breaking time t_{WB} , at which nonlinear nondispersive spreading leads to a gradient catastrophe; our approximation subsequently predicts a nonphysical multivalued profile, as can be seen in Fig. 3 (for $t > 20$). The time t_{WB} can be computed by noticing that the wave breaking occurs for the value $\lambda_{\text{WB}}^+ = (\rho_0 + \rho_1/\sqrt{e})^{1/2}$ which is associated in the initial profile with the largest gradient in $\partial_x \rho$. At the wave-breaking time the profile of λ^+ in region 3 has a vertical tangent line: $\partial x / \partial \lambda^+ = 0$. For simplicity we also assume that the wave breaking occurs in a region where one can safely approximate $\lambda^- = -c_0$. Differentiation of (7) then yields

$$t_{\text{WB}} = \frac{2}{3} \left| \frac{dW_+^{(3)}(-c_0, \lambda^+)}{d\lambda^+} \right|_{\lambda_{\text{WB}}^+} = \left| \frac{\int_{c_0}^{\lambda^+} \sqrt{r} w^\Lambda(r) dr}{\sqrt{2}(\lambda^+ + c_0)^{5/2}} + \frac{\sqrt{2}(c_0 - \lambda^+) w^\Lambda(\lambda^+)}{3\sqrt{\lambda^+}(\lambda^+ + c_0)^{3/2}} + \frac{2}{3} \sqrt{\frac{2\lambda^+}{\lambda^+ + c_0}} \frac{dw^\Lambda}{d\lambda^+} \right|_{\lambda_{\text{WB}}^+}. \quad (16)$$

The numerical value of t_{WB} is found to be $\simeq 19.15$ for our choice of initial condition, in good agreement with numerical simulations. Note also that for a small bump ($\rho_1 \ll \rho_0$) the wave breaking time becomes very large. From (16), and for an initial profile of type (2), one gets at leading order in ρ_1/ρ_0 :

$$t_{\text{WB}} \simeq \frac{2\sqrt{e} x_0}{3 c_0} \left(\frac{\rho_0}{\rho_1} \right). \quad (17)$$

This means that the breaking time is much greater than the time $\sim x_0/c_0$ of propagation of sound along the pulse profile. In our optical system the wave breaking is regularized by the formation of a dispersive

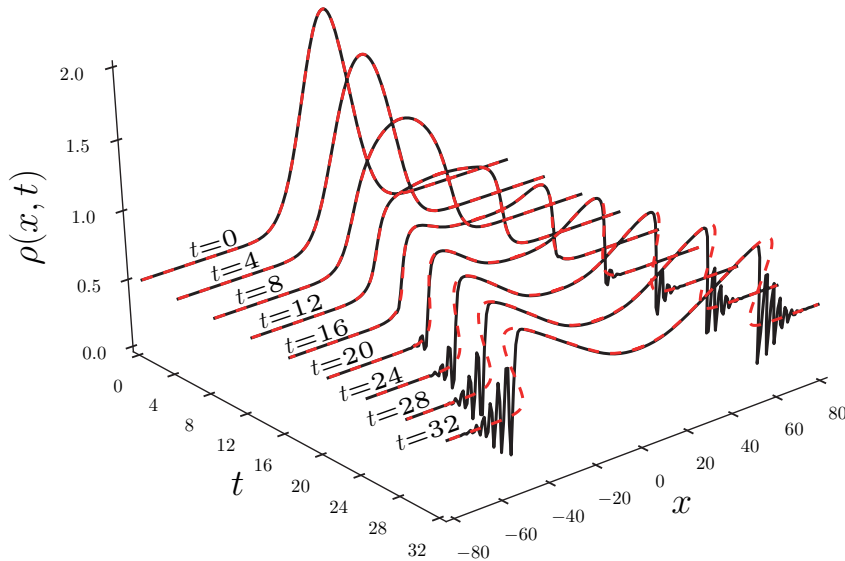


Figure 3. Density profile $\rho(x, t)$ corresponding to the initial conditions (2) with $\rho_0 = 0.5$, $\rho_1 = 1.5$ and $x_0 = 20$. The red dashed line corresponds to the exact solution of the dispersionless system (6) (see the text), while the black curve displays the density obtained from the numerical solution of Eq. (1).

shock wave which is a region with large oscillations of intensity and phase, whose extent increases with time, as can be seen in Fig. 3. Its description requires a nonlinear treatment able to account for dispersive effects and this goes beyond the scope of the present letter (see, e.g., Ref. [9]).

4 Conclusion

In this work we demonstrate that a nondispersive hydrodynamic approach to the spreading and splitting of an optical pulse compares extremely well with the results of numerical simulations up to the wave breaking time. At larger time, one observes the formation of an optical dispersive shock wave, which can be studied within Whitham modulation theory. In the case of the initial distribution given by Eq. (2), the shock should be described by four varying Riemann invariants and this requires a thorough investigation. Work in this direction is in progress.

References

1. V. I. TALANOV, *Radiophys.* **9**, 138 (1965).
2. S. A. AKHMANOV, A. P. SUKHORUKOV AND R. V. KHOKHLOV, *Usp. Fiz. Nauk* **93**, 19 (1967).
3. W. WAN, S. JIA, AND J. W. FLEISCHER, *Nature Phys.* **3**, 46 (2007).
4. L. D. LANDAU AND E. M. LIFSHITZ, *Electrodynamics of Continuous Media*, Course of Theoretical Physics vol. 8 (Elsevier Butterworth-Heinemann, Oxford, 2006).
5. A. M. KAMCHATNOV, *Nonlinear Periodic Waves and Their Modulations—An Introductory Course*, (World Scientific, Singapore, 2000).
6. S. P. TSAREV, *Math. USSR Izv.* **37**, 397 (1991).
7. A. SOMMERFELD, *Partial Differential Equations in Physics*, (Lectures on Theoretical Physics volume VI) (Academic Press, New York, 1964).
8. G. S. S. LUDFORD, *Proc. Camb. Phil. Soc.* **48**, 499 (1952).
9. M. ISOARD, A.M. KAMCHATNOV, N. PAVLOFF, arXiv:1902.06975 [nlin.PS] (2019).